

High-order mass- and energy-conserving methods for the nonlinear Schrödinger equation and its hyperbolization

Hendrik Ranocha^{*1} and David I. Ketcheson⁺²

¹Institute of Mathematics, Johannes Gutenberg University Mainz, Staudingerweg 9, 55128 Mainz, Germany

²King Abdullah University of Science and Technology (KAUST), Computer Electrical and Mathematical Science and Engineering Division (CEMSE), Thuwal, 23955-6900, Saudi Arabia

October 16, 2025

We propose a class of numerical methods for the nonlinear Schrödinger (NLS) equation that conserves mass and energy, is of arbitrarily high-order accuracy in space and time, and requires only the solution of a scalar algebraic equation per time step. We show that some existing spatial discretizations, including the popular Fourier spectral method, are in fact energy-conserving if one considers the appropriate form of the energy density. We develop a new relaxation-type approach for conserving multiple nonlinear functionals that is more efficient and robust for the NLS equation compared to the existing multiple-relaxation approach. The accuracy and efficiency of the new schemes is demonstrated on test problems for both the focusing and defocusing NLS.

Key words. additive Runge-Kutta methods, nonlinear Schrödinger equation, Gross-Pitaevskii equation, summation-by-parts operators, finite difference methods, Fourier collocation methods, structure-preserving methods

AMS subject classification. 65M12, 65M70, 65M06, 65M60, 65M20,

1 Introduction

We study discretizations of the nonlinear Schrödinger (NLS) equation (also referred to as Gross-Pitaevskii equation)

$$iu_t + u_{xx} + \beta|u|^2u = 0 \quad (1.1)$$

with periodic or homogeneous Neumann boundary conditions and given initial data $u(0, x) = u^0(x)$, where β is a real parameter. The case $\beta > 0$ is called focusing, while $\beta < 0$ is defocusing. The NLS equation arises in important physical applications, including deep water waves, Bose-Einstein condensates, and others. It is one of the most widely-studied examples of an integrable nonlinear

^{*}ORCID: 0000-0002-3456-2277

[†]ORCID: 0000-0002-1212-126X

PDE, and possesses a countably-infinite set of conserved functionals. Two of the most significant are the mass \mathcal{M} and energy \mathcal{E} :

$$\mathcal{M} := \int |u|^2 dx, \quad \mathcal{E} := \int \left(|u_x|^2 - \frac{\beta}{4} |u|^4 \right) dx. \quad (1.2)$$

For brevity, we will call a numerical scheme doubly-conservative if it conserves discrete analogs of both of the above quantities. Numerical conservation is extremely important in obtaining accurate solutions of (1.1). This is especially true when dealing with higher-degree nonlinearities or in higher dimensions, where it is possible for solutions to exhibit finite-time blowup, which depends critically on the value of the energy. In such cases, numerical conservation of the mass and energy is essential in order to obtain even qualitatively correct solutions. However, even conservative methods can struggle to accurately capture some solutions, such as multi-soliton bound states that exhibit large derivatives [38]. Thus, the ideal discretization would conserve the mass and energy and be high-order accurate while also being computationally efficient.

The earliest proposed doubly-conservative schemes were second-order accurate and fully implicit, requiring the solution of large systems of nonlinear algebraic equations [27, 72]. These methods have been analyzed later when combined with finite element schemes in space, e.g., [4, 37]. Sanz-Serna and Manoranjan proposed an explicit scheme that used a modified time step size to ensure fully-discrete conservation of the mass only [73]; that scheme can be seen as a precursor to the time relaxation approaches that have been developed more recently. Besse [12] proposed the first doubly-conservative scheme that does not require any nonlinear algebraic solve, as it is only linearly implicit; however, it is limited to second-order accuracy in time. The scalar auxiliary variable (SAV) approach has been used to conserve the mass and a modified energy with fully implicit methods [22]. Bai et al. [9] provided a family of conservative discretizations of arbitrarily high order in space and time, which require the use of fully-implicit time stepping. Akrivis et al. [3] propose a remarkable fully implicit class of schemes that conserve not only mass and energy, but also momentum. Biswas et al. [16] proposed an approach that couples existing mass- and momentum-conservative second-order spatial schemes with time relaxation in order to achieve fully-discrete conservation without the need to solve any large (linear or nonlinear) algebraic systems. If conservation is not required, then standard high-order time discretizations can be combined with spectral methods in space to obtain highly accurate schemes [7].

Among the existing approaches, we see that no scheme combines all of the following properties:

- Mass and energy conservation;
- Arbitrarily high order in space and time;
- No need to solve large algebraic systems of equations.

In the present work we propose such a class of methods for the NLS equation (1.1) in the presence of periodic or homogeneous Neumann boundary conditions. Furthermore, we provide new insight into some existing schemes that fit within the framework of summation-by-parts (SBP) spatial discretizations. In fact, we show that a broad class of schemes including the popular Fourier spectral discretization, previously thought to be only mass-preserving, are in fact also energy-preserving if one considers the appropriate form for the energy.

We formulate the mass- and energy-conserving spatial semidiscretizations using SBP operators in Section 2. References and introductions to SBP operators are given in [32, 77]. SBP operators can be used to formulate finite differences (FDs) [21, 49, 74], finite volumes [58], continuous Galerkin (CG) finite elements [2, 40, 41], discontinuous Galerkin (DG) methods [20, 34], flux reconstruction (FR) [42, 66, 78], active flux methods [11, 31], as well as meshless schemes [39].

To construct high-order accurate time integrators that conserve mass and energy in Section 3, we extend the recently developed framework of relaxation-in-time methods [47, 64, 68]. The basis for these methods goes back to [71] and [26, pp. 265–266]. It has been used for various time integration

schemes, e.g., Runge-Kutta methods [68], linear multistep methods [64], residual distribution schemes [1], IMEX methods [45, 53], and multi-derivative methods [69, 70]. Applications include among others Hamiltonian problems [52, 62, 80], kinetic equations [51], compressible flows [29, 61, 79], and dispersive wave equations [50, 54, 57, 67].

In Section 4, we compare the performance of our proposed approach to other methods from the literature, demonstrating that it is faster in all cases tested. In Section 5, we develop similar semidiscretizations for the hyperbolized NLS equation [15] and combine them with the new time integrators. Finally, we summarize and discuss our findings in Section 6.

We have implemented all methods in Julia [14] using `SummationByPartsOperators.jl` [60] for the spatial semidiscretizations, wrapping `FFTW.jl` [33] for the Fourier collocation methods. To solve sparse linear systems, we use `UMFPACK` from `SuiteSparse` [6, 24, 25] wrapped in the Julia standard library. To solve the nonlinear relaxation equation, we use the method of [48] implemented in `SimpleNonlinearSolve.jl` [59]. We use `CairoMakie.jl` [23] to visualize the results. All code and data required to reproduce the numerical results is available online [63].

2 Spatial semidiscretizations

We start by recalling two well-known spatial discretizations with conservation properties. As we will see, both of these fit into a broader framework of SBP discretizations, which we then introduce and discuss more generally. The main theoretical contribution of this section is the arbitrarily high-order accurate mass- and energy-conserving semidiscretizations introduced in Section 2.3.

Separating the real and imaginary parts of $u = v + iw$, we can rewrite (1.1) as

$$\begin{aligned} v_t + w_{xx} + \beta(v^2 + w^2)w &= 0, \\ w_t - v_{xx} - \beta(v^2 + w^2)v &= 0. \end{aligned} \tag{2.1}$$

Given a spatial interval $[x_L, x_R]$, we consider (possibly non-uniform) grids $\mathbf{x} = (x_1, \dots, x_N)^T$ with $x_L = x_1 \leq \dots$ and $x_N = x_R$ for non-periodic boundary conditions; for periodic boundaries, x_N may not coincide with x_R . We specifically allow $x_i = x_{i+1}$ for some i to formulate discontinuous Galerkin methods naturally as SBP methods. Furthermore, we consider collocation methods, i.e., the numerical solution is represented by point values $\mathbf{u} = (u_1, \dots, u_N)^T$ with $u_i \approx u(x_i)$.

2.1 Two examples of conservative semidiscretizations

For the NLS equation (2.1) with periodic boundaries, perhaps the most widely used spatial discretization is based on Fourier collocation spectral differentiation, wherein the second-derivative operator ∂_{xx} is approximated on a uniform grid in space by a symmetric operator related to the discrete Fourier transform on a uniform grid. Semidiscretizations based on this are known to preserve the discrete mass (see e.g. [10]) which is given by

$$\mathcal{M} = \mathbf{v}^T M \mathbf{v} + \mathbf{w}^T M \mathbf{w} \approx \int (v^2 + w^2) dx = \int |u|^2 dx \tag{2.2}$$

where \mathbf{v}, \mathbf{w} are the real and imaginary parts of \mathbf{u} , respectively, and $M = \Delta x \mathbf{I}$ is the mass matrix obtained by multiplying the identity matrix \mathbf{I} by the grid spacing $\Delta x = x_{i+1} - x_i$.

Next we consider a second-order-accurate finite element discretization that conserves both discrete mass (2.2) and the energy functional

$$\begin{aligned} \mathcal{E} &= \Delta x \sum_{i=1}^{N-1} \left(\frac{(v_{i+1} - v_i)^2}{\Delta x^2} + \frac{(w_{i+1} - w_i)^2}{\Delta x^2} \right) - \frac{\beta}{2} \mathbf{1}^T M (\mathbf{v}^2 + \mathbf{w}^2)^2 \\ &\approx \int \left((v_x)^2 + (w_x)^2 - \frac{\beta}{2} (v^2 + w^2)^2 \right) = \int \left(|u_x|^2 - \frac{\beta}{2} |u|^4 \right). \end{aligned} \tag{2.3}$$

The scheme is [38]

$$\mathbf{v}'(t) = M^{-1} A_2 \mathbf{w} - \beta(\mathbf{v}^2 + \mathbf{w}^2) \mathbf{w}, \quad (2.4)$$

$$\mathbf{w}'(t) = -M^{-1} A_2 \mathbf{v} + \beta(\mathbf{v}^2 + \mathbf{w}^2) \mathbf{v}, \quad (2.5)$$

where for homogeneous Neumann boundaries, the matrices M and A_2 are given by

$$M = \Delta x \begin{pmatrix} \frac{1}{2} & & & \\ & 1 & & \\ & & \ddots & \\ & & & 1 \\ & & & & \frac{1}{2} \end{pmatrix}, \quad A_2 = \frac{1}{\Delta x} \begin{pmatrix} 1 & -1 & & \\ -1 & 2 & -1 & \\ & \ddots & \ddots & \ddots \\ & & -1 & 2 & -1 \\ & & & -1 & 1 \end{pmatrix}. \quad (2.6)$$

Both of the above semidiscretizations approximate the second derivative using a symmetric matrix, and each of these matrices, combined with the corresponding mass matrix (given by the scaled identity $M = \Delta x \mathbf{I}$ for the spectral method and by M in (2.6) for the finite element method), satisfy what is known as a summation-by-parts (SBP) property.

2.2 Summation-by-parts operators

In this section we review standard SBP operators and notation; for more details see e.g. [32, 55, 56, 65, 77]. In non-periodic domains, the restriction of a numerical solution \mathbf{u} to the boundaries is given by $\mathbf{t}_L^T \mathbf{u}$ and $\mathbf{t}_R^T \mathbf{u}$, where

$$\mathbf{t}_L = (1, 0, \dots, 0)^T, \quad \mathbf{t}_R = (0, \dots, 0, 1)^T. \quad (2.7)$$

For periodic domains, we use the convention $\mathbf{t}_L = \mathbf{t}_R = \mathbf{0}$ to simplify the notation.

Definition 2.1. A first-derivative SBP operator on the grid \mathbf{x} is given by a consistent first-derivative operator $D_1 \in \mathbb{R}^{N \times N}$ and a symmetric and positive definite mass/norm matrix $M \in \mathbb{R}^{N \times N}$ satisfying the SBP property

$$MD_1 + D_1^T M = \mathbf{t}_R \mathbf{t}_R^T - \mathbf{t}_L \mathbf{t}_L^T, \quad (2.8)$$

where $\mathbf{t}_L, \mathbf{t}_R \in \mathbb{R}^N$ are the boundary restriction operators described above. \triangleleft

Definition 2.2. First-derivative upwind SBP operators on the grid \mathbf{x} are given by consistent first-derivative operators $D_{\pm} \in \mathbb{R}^{N \times N}$ and a symmetric and positive definite mass/norm matrix $M \in \mathbb{R}^{N \times N}$ satisfying the upwind SBP property

$$MD_+ + D_-^T M = \mathbf{t}_R \mathbf{t}_R^T - \mathbf{t}_L \mathbf{t}_L^T, \quad M(D_+ - D_-) \text{ is symmetric and negative semidefinite}, \quad (2.9)$$

where $\mathbf{t}_L, \mathbf{t}_R \in \mathbb{R}^N$ are the boundary restriction operators described above. \triangleleft

Definition 2.3. A second-derivative SBP operator on the grid \mathbf{x} is given by a consistent second-derivative operator $D_2 \in \mathbb{R}^{N \times N}$ and a symmetric and positive definite mass/norm matrix $M \in \mathbb{R}^{N \times N}$ satisfying the SBP property

$$MD_2 = \mathbf{t}_R \mathbf{d}_R^T - \mathbf{t}_L \mathbf{d}_L^T - A_2, \quad A_2 \text{ is symmetric and negative semidefinite}, \quad (2.10)$$

where $\mathbf{t}_L, \mathbf{t}_R \in \mathbb{R}^N$ are the boundary restriction operators described above and $\mathbf{d}_L, \mathbf{d}_R \in \mathbb{R}^N$ yield consistent first-derivative approximations at the boundaries. \triangleleft

It can be verified by direct computation that both of the semidiscretizations described in Section 2.1 satisfy the conditions of Definition 2.3.

In the following, we will only use diagonal mass/norm matrices M . Concretely, we will use FDs, CG spectral element methods, DG spectral element methods, and Fourier collocation schemes. See, e.g., [65] for details and additional references.

2.3 A general doubly-conservative SBP semidiscretization

We propose the general SBP semidiscretization

$$\begin{aligned}\partial_t \mathbf{v} &= -(D_2 - M^{-1} \mathbf{t}_R \mathbf{d}_R^T + M^{-1} \mathbf{t}_L \mathbf{d}_L^T) \mathbf{w} - \beta(\mathbf{v}^2 + \mathbf{w}^2) \mathbf{w}, \\ \partial_t \mathbf{w} &= (D_2 - M^{-1} \mathbf{t}_R \mathbf{d}_R^T + M^{-1} \mathbf{t}_L \mathbf{d}_L^T) \mathbf{v} + \beta(\mathbf{v}^2 + \mathbf{w}^2) \mathbf{v},\end{aligned}\quad (2.11)$$

of the nonlinear Schrödinger equation (2.1), where D_2 is a second-derivative SBP operator with diagonal mass matrix M . Recall that we use the convention $\mathbf{t}_L = \mathbf{t}_R = \mathbf{d}_L = \mathbf{d}_R = \mathbf{0}$ in periodic domains and abbreviate

$$D_2 - M^{-1} \mathbf{t}_R \mathbf{d}_R^T + M^{-1} \mathbf{t}_L \mathbf{d}_L^T = -M^{-1} A_2. \quad (2.12)$$

For CG spectral element methods with homogeneous Neumann boundary conditions on a uniform mesh, this SBP semidiscretization is exactly (2.4). For Fourier collocation methods, it is the standard semidiscretization using the Fourier spectral second-derivative operator described in Section 2.1.

In order to discuss the energy conservation property for (2.11), we introduce a different form of the discrete energy:

$$\begin{aligned}\mathcal{E} &= \mathbf{v}^T A_2 \mathbf{v} + \mathbf{w}^T A_2 \mathbf{w} - \frac{\beta}{2} \mathbf{1}^T M (\mathbf{v}^2 + \mathbf{w}^2)^2 \\ &\approx \int \left((v_x)^2 + (w_x)^2 - \frac{\beta}{2} (\mathbf{v}^2 + \mathbf{w}^2)^2 \right) = \int \left(|u_x|^2 - \frac{\beta}{2} |u|^4 \right).\end{aligned}\quad (2.13)$$

In fact, (2.3) is of the form (2.13) since

$$\begin{aligned}\sum_{i=1}^{N-1} (v_{i+1} - v_i)^2 &= \sum_{i=1}^{N-1} (v_{i+1}^2 - 2v_i v_{i+1} + v_i^2) = v_1^2 + 2 \sum_{i=2}^{N-1} v_i^2 + v_N^2 - 2 \sum_{i=1}^{N-1} v_i v_{i+1} \\ &= v_1^2 + 2 \sum_{i=2}^{N-1} v_i^2 + v_N^2 - \sum_{i=1}^{N-1} v_i v_{i+1} - \sum_{i=2}^N v_i v_{i-1} \\ &= \sum_{i=2}^{N-1} v_i (-v_{i+1} + 2v_i - v_{i-1}) + v_1(v_1 - v_2) + v_N(v_N - v_{N-1}) = \Delta x \mathbf{v}^T A_2 \mathbf{v}.\end{aligned}\quad (2.14)$$

The form (2.13) using the discrete second-derivative operator can be generalized more easily to general SBP operators. Thus, we will use (2.13) in the following. We will see in Section 2.4 that this choice of the discrete total energy is crucial.

Theorem 2.4. *The semidiscretization (2.11) conserves the discrete total mass \mathcal{M} (2.2) and the discrete total energy \mathcal{E} (2.13) for diagonal-norm SBP operators.*

Proof. Since the mass matrix M is symmetric, we have

$$\begin{aligned}\partial_t \mathcal{M} &= 2\mathbf{v}^T M \partial_t \mathbf{v} + 2\mathbf{w}^T M \partial_t \mathbf{w} \\ &= -2\mathbf{v}^T A_2 \mathbf{w} - 2\beta \mathbf{v}^T M (\mathbf{v}^2 + \mathbf{w}^2) \mathbf{w} + 2\mathbf{w}^T A_2 \mathbf{v} + 2\beta \mathbf{w}^T M (\mathbf{v}^2 + \mathbf{w}^2) \mathbf{v} = 0,\end{aligned}\quad (2.15)$$

where we have used the symmetry of A_2 and the fact that the mass matrix M is diagonal. For the energy, we compute

$$\begin{aligned}\partial_t \mathcal{E} &= 2\mathbf{v}^T A_2 \partial_t \mathbf{v} + 2\mathbf{w}^T A_2 \partial_t \mathbf{w} - 2\beta \mathbf{1}^T M (\mathbf{v}^2 + \mathbf{w}^2) \mathbf{v} \partial_t \mathbf{v} - 2\beta \mathbf{1}^T M (\mathbf{v}^2 + \mathbf{w}^2) \mathbf{w} \partial_t \mathbf{w} \\ &= 2\mathbf{v}^T A_2 M^{-1} A_2 \mathbf{w} - 2\beta \mathbf{v}^T A_2 (\mathbf{v}^2 + \mathbf{w}^2) \mathbf{w} - 2\mathbf{w}^T A_2 M^{-1} A_2 \mathbf{v} \\ &\quad + 2\beta \mathbf{w}^T A_2 (\mathbf{v}^2 + \mathbf{w}^2) \mathbf{v} - 2\beta \mathbf{1}^T (\mathbf{v}^2 + \mathbf{w}^2) \mathbf{v} A_2 \mathbf{w} + 2\beta^2 \mathbf{1}^T M (\mathbf{v}^2 + \mathbf{w}^2)^2 \mathbf{v} \mathbf{w} \\ &\quad + 2\beta \mathbf{1}^T (\mathbf{v}^2 + \mathbf{w}^2) \mathbf{w} A_2 \mathbf{v} - 2\beta^2 \mathbf{1}^T M (\mathbf{v}^2 + \mathbf{w}^2)^2 \mathbf{v} \mathbf{w} \\ &= 0,\end{aligned}\quad (2.16)$$

where we have again used the symmetry of A_2 and the fact that the mass matrix M is diagonal. \square

2.4 Importance of the kinetic energy discretization

It is crucial to choose the discretization of the kinetic energy using the second-derivative SBP operator as in (2.13). To demonstrate this, we consider the two-soliton setup described in [16] and discretize it with a Fourier collocation method using N nodes. We compute the absolute changes of the total mass (2.2), the total energy (2.13) (computed correctly using the second-derivative SBP operator), and a naive version of the total energy where the kinetic energy terms are computed as

$$\mathbf{v}^T D_1^T M D_1 \mathbf{v} \approx \int |v_x|^2, \quad (2.17)$$

where $M = \Delta x \mathbf{I}$ is the usual Fourier collocation mass matrix and D_1 the corresponding first-derivative operator.

The second-derivative FFT-based operator D_2 is the same as the square of the first-derivative FFT-based operator D_1 if and only if the number of nodes N is odd [43]. Thus, we expect to see some clear differences for even N (which is usually chosen in practice for efficiency) but not for odd N (which is rarely used in practice, if at all).

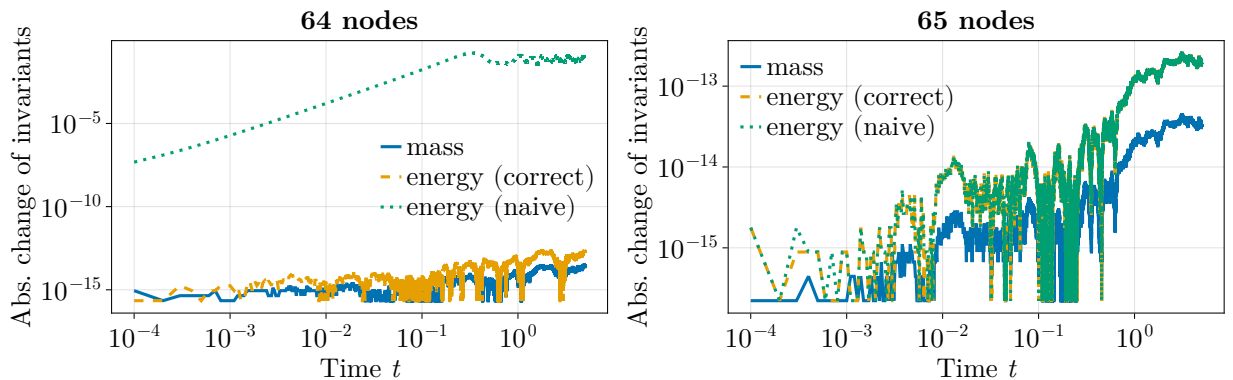


Figure 1: Absolute changes of the discretized invariants of the nonlinear Schrödinger equation for Fourier collocation methods with $N \in \{64, 65\}$ nodes in the domain $[-35, 35]$ for the two-soliton setup. The semidiscretization is integrated in time with the fifth-order method of [46] and time step size $\Delta t = 10^{-4}$.

The results shown in Figure 1 support the theoretical prediction. Indeed, the total mass and the correctly discretized total energy are conserved up to the error of the time integrator, which is close to machine precision due to sufficiently small time step sizes to highlight the spatial effects. In contrast, the naive discretization of the total energy varies significantly.

2.5 Numerical verification of the semidiscrete invariant conservation

Having verified the mass and energy conservation for Fourier collocation methods, we next demonstrate these structure-preserving properties for FD, CG, and local DG (LDG) SBP operators in periodic and bounded domains. As in Section 2.4, we choose the two-soliton setup, coarse spatial resolutions, and highly resolved time discretizations. The results shown in Figure 2 support the analysis, i.e., the total mass and the total energy are conserved up to a small error caused by the time integrator.

2.6 Convergence tests in space

Next, we use the two-soliton setup again to verify the high-order accuracy of the spatial semidiscretizations. We choose a sufficiently small time step size $\Delta t = 5 \times 10^{-5}$ to make sure that the error is dominated by the spatial discretization.

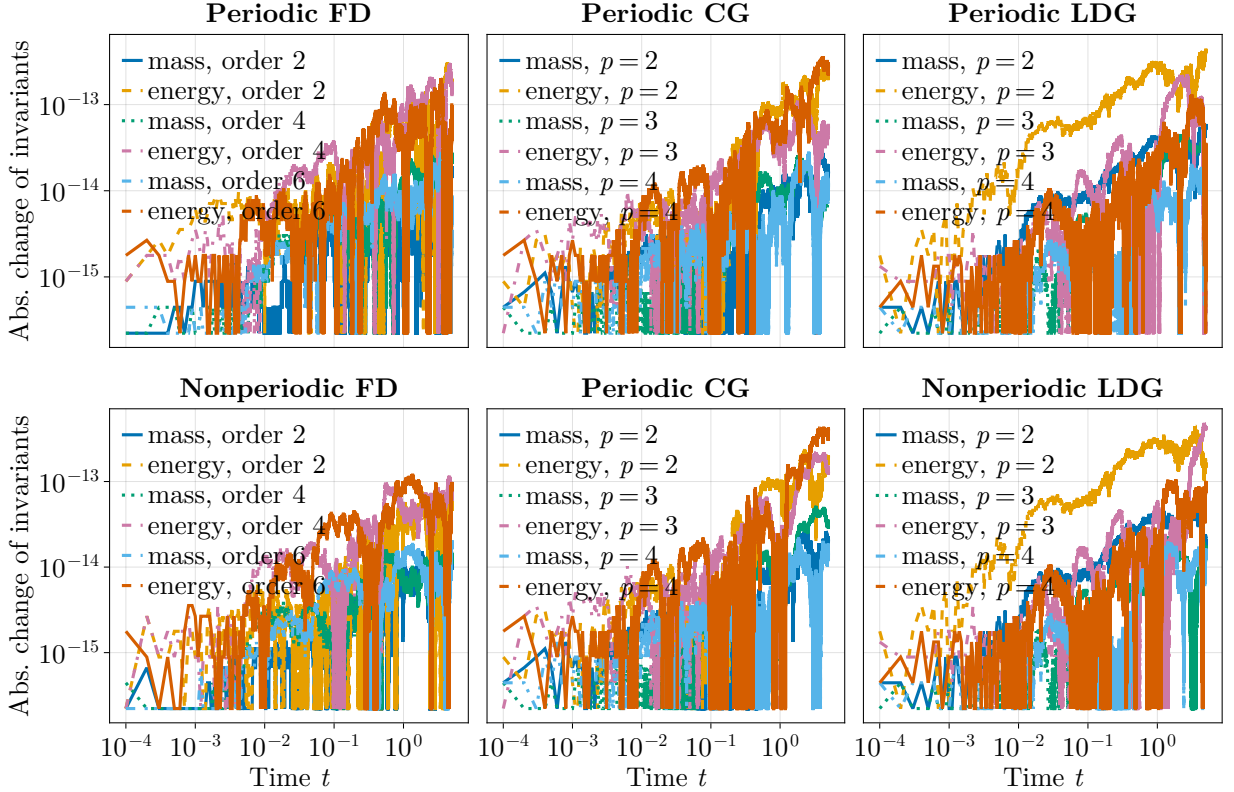


Figure 2: Absolute changes of the discretized invariants of the nonlinear Schrödinger equation for the two-soliton setup. The semidiscretizations are integrated in time with the fifth-order method of [46] and time step size $\Delta t = 10^{-4}$. For all semidiscretizations, we use approximately 64 degrees of freedom with slight deviations depending on the polynomial degree p for Galerkin methods.

The results shown in Figure 3 confirm the high accuracy of the spatial semidiscretizations. For all methods, we measured the error in the discrete L^2 norm induced by the (diagonal) mass matrix M . For periodic finite differences, we observe the expected order of convergence determined by the order of accuracy. For finite differences with homogeneous Neumann boundary conditions, we also observe the same order of convergence, although SBP operators typically lead to a reduced order of convergence due to the lower order of accuracy at the boundaries [75, 76]. However, we have chosen the domains large enough so that the interaction with the boundaries is negligible (since the soliton solutions are only valid on the whole real line).

Both CG and DG methods show a superconvergence rate between $2p$ and $2p + 1/2$, where p is the polynomial degree. Superconvergence effects like this have been observed and studied for Galerkin-type methods in several cases, e.g., [19, 30].

2.7 Dispersive shock wave

Next, we consider a dispersive shock wave for the defocusing NLS with $\beta = -1$ following [28, 35]. We use a smoothed Riemann problem as initial condition:

$$\varrho = \frac{\varrho_L + \varrho_R}{2} + \frac{\varrho_R - \varrho_L}{2} \tanh(100x), \quad \theta = 0, \quad (2.18)$$

where the hydrodynamic variables ϱ and θ are related to u via the Madelung transformation

$$u = \sqrt{\varrho} \exp(i\theta). \quad (2.19)$$

As in [28, Section 5.2], we use the parameters $\varrho_L = 2$ and $\varrho_R = 1$.

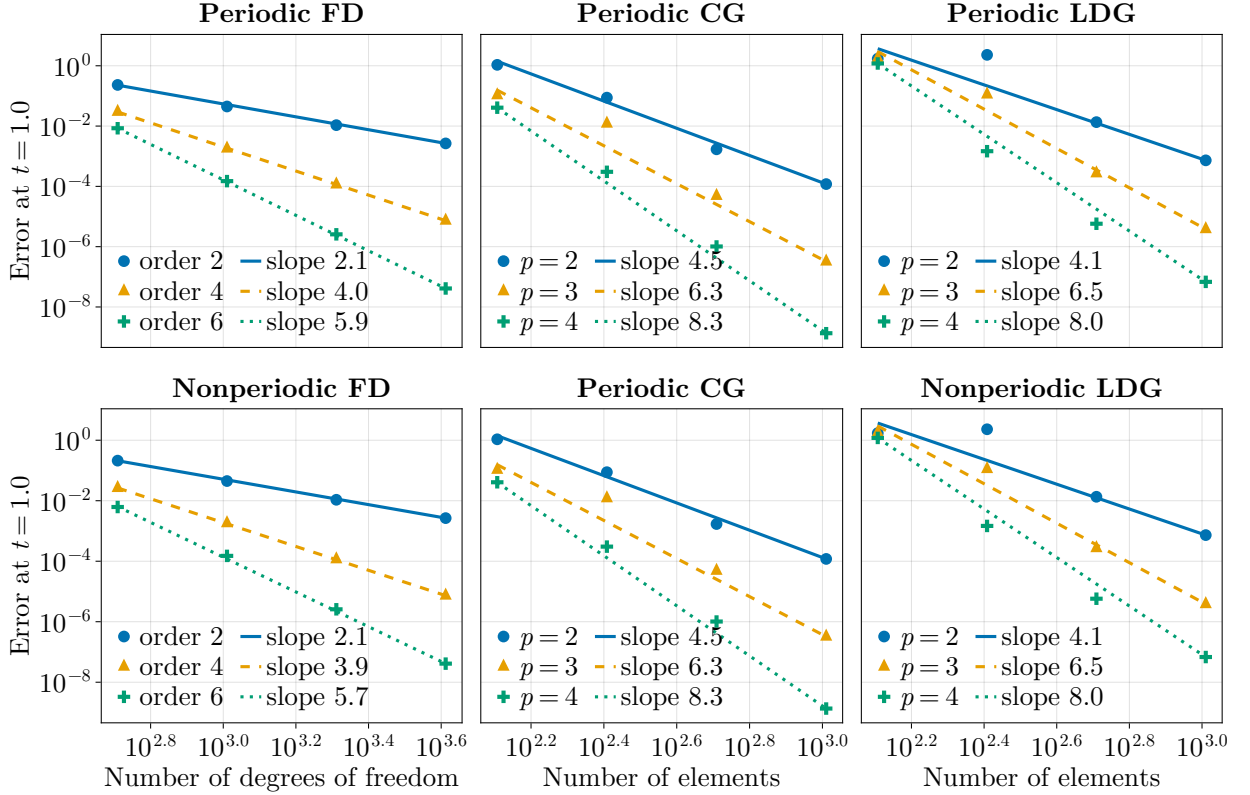


Figure 3: Spatial convergence study for the two-soliton setup. The semidiscretizations are integrated in time with the fifth-order method of [46] and time step size $\Delta t = 5 \times 10^{-5}$. For finite difference methods, the “order” refers to the order of accuracy in the interior. For Galerkin methods, p is the polynomial degree.

To avoid interactions with the boundaries while focusing on the dispersive shock wave, we consider the large domain $[-1600, 1600]$ and show the numerical solution at time $t = 100$ for $-400 < x < 500$. We use Fourier collocation methods with $N = 2^{16}$ nodes in space and the fifth-order method of [46] with time step size $\Delta t = 0.05$. To plot the hydrodynamic variables $\varrho = |u|^2$ and $v = \theta_x$, we compute the argument of u using the two-argument arc tangent, correct branch cuts, and differentiate the result numerically.

The results shown in Figure 4 are in good agreement with the numerical and analytical results of [28]. In particular, the asymptotic values ϱ_L , ϱ_R , and $v_L = 0 = v_R$ as well as the intermediate state (ϱ_0, v_0) are captured correctly. Furthermore, the extent of the waves in the self-similarity variable $\xi = x/t$ agrees well with the theoretical predictions based on Whitham’s modulation equations [28, Section 2.2.2].

3 Time discretizations

Many differential equations possess one or more linear invariants, and these are automatically preserved by Runge-Kutta and multistep methods. In order to also preserve a nonlinear invariant, one can use orthogonal projection (see e.g. [36, Section IV.4]) or relaxation (see e.g. [64]). However, orthogonal projection is problematic in that setting because it destroys the linear invariant. Relaxation is advantageous in this case and can be viewed as an oblique projection, along a line that is known to conserve linear invariants.

In this section we propose a quadratic-preserving relaxation method, analogous to the linear-preserving relaxation method just mentioned. It performs a projection or line search along a curve

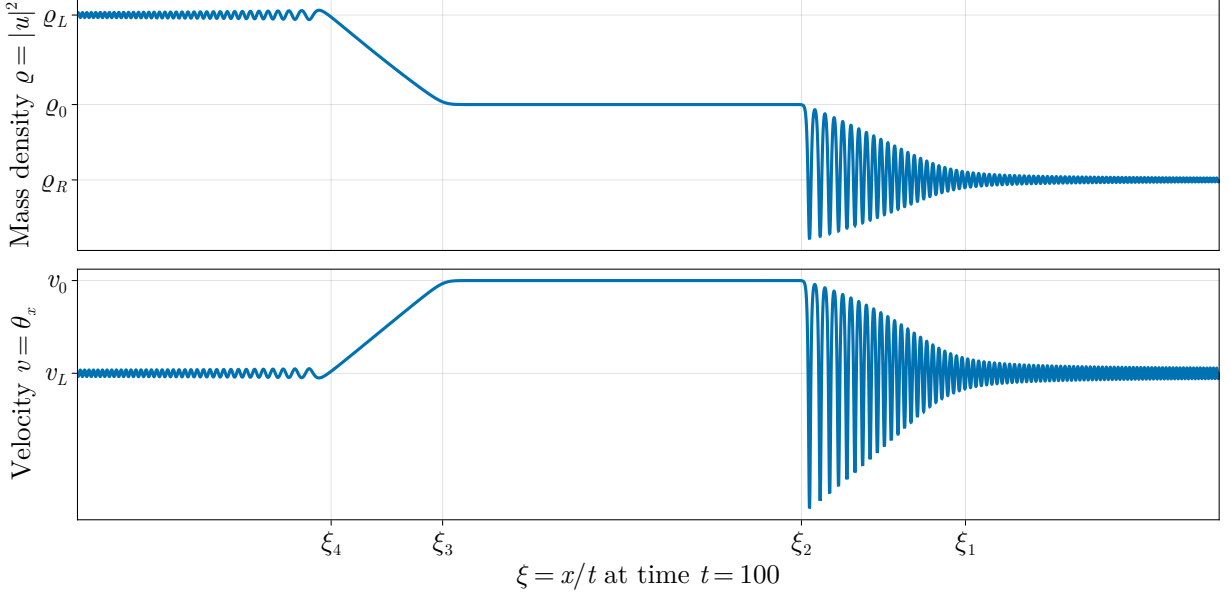


Figure 4: Numerical results for the dispersive shock wave obtained with Fourier collocation methods and the fifth-order method of [46].

known to preserve one simple (in this case quadratic) invariant, in order to find a solution that also preserves a second nonlinear invariant. Due to the simplicity of projecting onto a quadratic invariant manifold, this leads to an efficient and robust algorithm and avoids the need to solve more than one nonlinear algebraic equation, as was required with the multiple relaxation approach in [16, 17].

3.1 Quadratic-preserving relaxation

Consider an ODE

$$\frac{d}{dt}u(t) = f(u(t)) \quad (3.1)$$

with invariant (first integral) η , i.e.,

$$\forall u: \quad \eta'(u)f(u) = 0. \quad (3.2)$$

Relaxation one-step methods [47, 64, 68] perform the following steps to conserve η :

- Given $u^n \approx u(t^n)$, compute a provisional value $\tilde{u}^{n+1} \approx u(\tilde{t}^{n+1})$ using a standard one-step method, where $\tilde{t}^{n+1} = t^n + \Delta t$.
- Solve the scalar equation
$$\eta(u^n + \gamma(\tilde{u}^{n+1} - u^n)) = \eta(u^n) \quad (3.3)$$
for the scalar relaxation parameter γ .
- Continue the integration with

$$u^{n+1} = u^n + \gamma(\tilde{u}^{n+1} - u^n) \approx u(t^{n+1}), \quad t^{n+1} = t^n + \gamma\Delta t, \quad (3.4)$$

instead of \tilde{u}^{n+1} and \tilde{t}^{n+1} .

The available theory guarantees that there is a unique solution $\gamma = 1 + O(\Delta t^{p-1})$ under a certain non-degeneracy condition, where $p \geq 2$ is the order of the baseline method; in this case, the relaxed method is also at least p -th order accurate [47, 64, 68].

By construction, the relaxed method conserves the invariant η and also all linear invariants conserved by the baseline method, i.e., all linear invariants of the ODE for general linear methods such as Runge-Kutta methods. Since the NLS has no linear invariants but two nonlinear invariants (mass and energy) that are conserved by the spatial discretizations introduced in Section 2, we generalize the relaxation approach to this setting. Instead of searching for a solution conserving the invariant η along the secant line connecting u^n and \tilde{u}^{n+1} , we propose to perform the search along the geodesic line connecting u^n and \tilde{u}^{n+1} on the manifold defined by the total mass, i.e., a sphere. By construction, this approach conserves the total mass and the total energy.

To describe the method, we consider a slightly more general setting. Assume that we have an ODE (3.1) with two invariants η and μ . Moreover, assume that the projection onto the manifold defined by the invariant μ is given by the (general, non-linear) projection operator π . The new quadratic-preserving relaxation method performs the following steps:

1. Given $u^n \approx u(t^n)$, compute a provisional value $\tilde{u}^{n+1} \approx u(\tilde{t}^{n+1})$ using a standard one-step method, where $\tilde{t}^{n+1} = t^n + \Delta t$.
2. Project the provisional value onto the manifold defined by the projection operator π :

$$\hat{u}^{n+1} = \pi(\tilde{u}^{n+1}). \quad (3.5)$$

3. Solve the scalar equation

$$\eta\left(\pi(u^n + \gamma(\hat{u}^{n+1} - u^n))\right) = \eta(u^n) \quad (3.6)$$

for the scalar relaxation parameter γ .

4. Continue the integration with

$$u^{n+1} = \pi(u^n + \gamma(\hat{u}^{n+1} - u^n)) \approx u(t^{n+1}), \quad t^{n+1} = t^n + \gamma\Delta t, \quad (3.7)$$

instead of \tilde{u}^{n+1} and \tilde{t}^{n+1} .

For the nonlinear Schrödinger equation, the projection operator π is the projection onto the sphere defined by the total mass, i.e.,

$$\pi(\tilde{u}^{n+1}) = \sqrt{\frac{\mathcal{M}(u^n)}{\mathcal{M}(\tilde{u}^{n+1})}} \tilde{u}^{n+1}. \quad (3.8)$$

This approach is justified by the following theorem.

Theorem 3.1. *Assume that the ODE (3.1) has the invariants (η, μ) and that π is the projection operator onto the manifold defined by the invariant μ . Moreover, assume that the baseline one-step method is of order $p \geq 2$ and that*

$$\eta'(u^n)\pi'(u^n)f'(u^n)f(u^n) \neq 0. \quad (3.9)$$

Then, the quadratic-preserving relaxation method described above is well-defined for sufficiently small time step sizes Δt ; there is a unique solution $\gamma = 1 + \mathcal{O}(\Delta t^{p-1})$ and the quadratic-preserving relaxation method is at least of order p (when measuring the error at the relaxed time t^{n+1}). Moreover, it conserves both invariants η and μ .

Remark 3.2. The non-degeneracy condition (3.9) is the same as for standard relaxation methods if $\pi = \text{id}$ is the identity. It guarantees, for example, that u^n is not a steady state of the ODE (in which case the baseline method would not change the solution and γ would be undefined). Since $\eta(\pi(u)) \equiv \text{const}$, we have

$$\eta'\pi'f = 0, \quad \eta''(\pi'f, f) + \eta'\pi''(f, f) + \eta'\pi'f'f = 0. \quad (3.10)$$

Hence, for $\pi = \text{id}$, the non-degeneracy condition (3.9) is equivalent to $\eta'f'f = -\eta''(f, f) \neq 0$. This is satisfied, for example, if η is strictly convex and $f(u^n) \neq 0$. \triangleleft

Proof of Theorem 3.1. The proof is based on the implicit function theorem, similar to proofs for standard projection and relaxation methods, e.g., [18, Theorem 2], [68, Proposition 2.18], and [64, Theorem 2.14]. Consider the residual

$$\eta\left(\pi(u^n + \gamma(\hat{u}^{n+1} - u^n))\right) - \eta(u^n), \quad (3.11)$$

which needs to be zero for the desired relaxation parameter γ . Writing $\gamma = 1 + \delta\Delta t^{p-2}$, we can formulate this as the equivalent problem of finding a root δ of

$$r(\Delta t, \delta) = \Delta t^{-p} \left(\eta\left(\pi(\hat{u}^{n+1} + \delta\Delta t^{p-2}(\hat{u}^{n+1} - u^n))\right) - \eta(u^n) \right) \quad (3.12)$$

depending on Δt . Since the baseline method is p -th order accurate, we have

$$\eta\left(\pi(\hat{u}^{n+1} + \delta\Delta t^{p-2}(\hat{u}^{n+1} - u^n))\right) - \eta(u^n) = O(\Delta t^{p+1}), \quad (3.13)$$

if $\delta = O(\Delta t)$, since the argument of π is a p -th order approximation of $u(t^n + \gamma\Delta t)$, see [64, Lemma 2.7]. Thus,

$$r(\Delta t = 0, \delta = 0) = 0. \quad (3.14)$$

Moreover, we compute

$$\begin{aligned} \partial_\delta r(\Delta t, \delta) &= \Delta t^{-2} \eta' \left(\pi(\hat{u}^{n+1} + \delta\Delta t^{p-2}(\hat{u}^{n+1} - u^n)) \right) \\ &\quad \pi'(\hat{u}^{n+1} + \delta\Delta t^{p-2}(\hat{u}^{n+1} - u^n))(\hat{u}^{n+1} - u^n). \end{aligned} \quad (3.15)$$

Since the baseline method is at least second-order accurate, we have

$$\hat{u}^{n+1} - u^n = \Delta t f(u^n) + \frac{\Delta t^2}{2} f'(u^n) f(u^n) + O(\Delta t^3). \quad (3.16)$$

Moreover, since $\eta(\pi(u)) \equiv \text{const}$, we have $\eta' \pi' f = 0$. Thus,

$$\partial_\delta r(\Delta t = 0, \delta = 0) = \eta'(u^n) \pi'(u^n) f'(u^n) f(u^n) \neq 0 \quad (3.17)$$

by the non-degeneracy condition (3.9). Thus, the implicit function theorem guarantees that there is a unique solution $\delta = O(\Delta t)$ of $r(\Delta t, \delta) = 0$ for sufficiently small Δt . This implies the existence of a unique solution $\gamma = 1 + \delta\Delta t^{p-2} = 1 + O(\Delta t^{p-1})$. The order of accuracy of the quadratic-preserving relaxation method follows from [64, Lemma 2.7]. \square

3.2 Numerical verification of the fully-discrete invariant conservation

To visualize the influence of the mass- and energy-preserving relaxation method in time, we consider both the two-soliton and the three-soliton setups described in [16]. We use Fourier collocation methods with $N = 2^{10}$ nodes in the domain $[-35, 35]$ for the spatial semidiscretization and the third-order method of [8] for the time discretization. Following [16], we visualize the numerical solutions with and without relaxation at time $t = 4.3$.

The results shown in Figure 5 confirm the advantages of using relaxation to conserve mass and energy. In particular, both mass and energy are preserved up to the error of the nonlinear solver (which is close to machine precision). While the baseline method without relaxation does not capture the correct solution with the chosen time step sizes, the relaxed solutions are visually indistinguishable from the exact solutions.

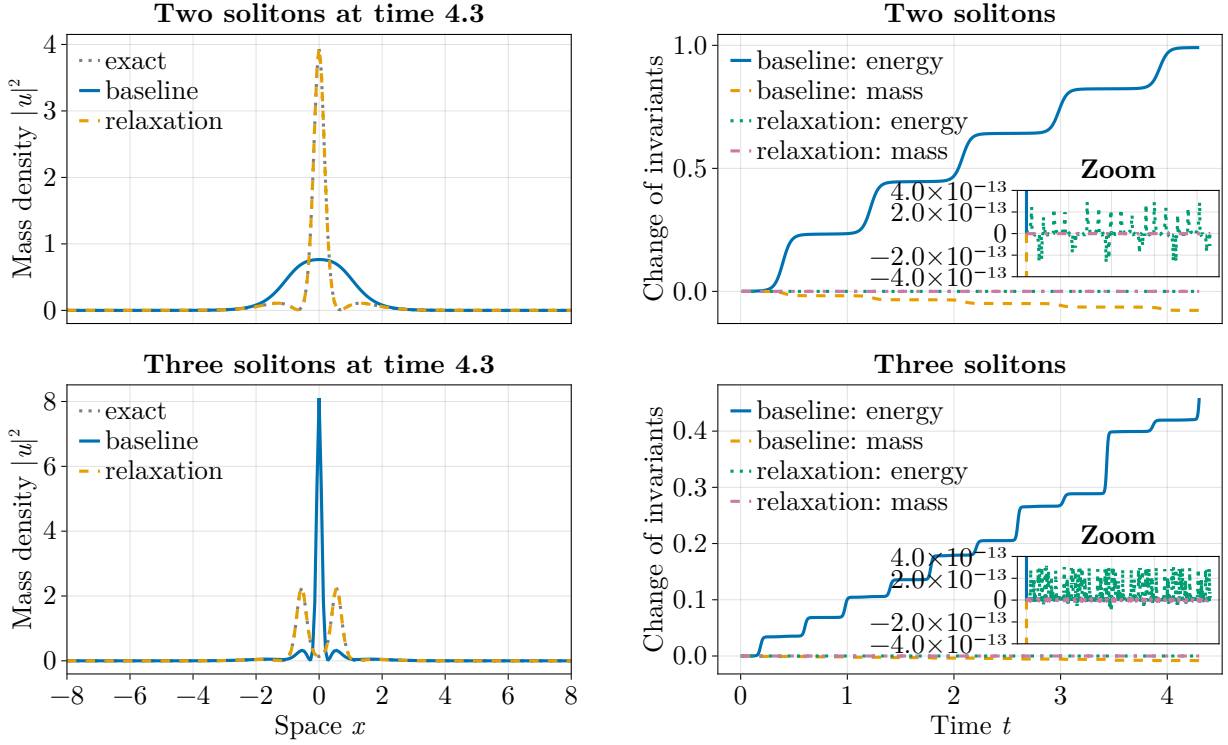


Figure 5: Numerical results obtained for the two- ($\Delta t = 10^{-2}$) and three-soliton ($\Delta t = 10^{-3}$) setups using Fourier collocation methods with $N = 2^{10}$ nodes in the domain $[-35, 35]$ in space and the third-order method of [8] in time.

3.3 Convergence tests in time

Next, we verify the high-order accuracy of the time discretizations with and without relaxation to conserve mass and energy. Similar to [16], we consider both the two-soliton and the three-soliton setup, since the one-soliton setup is easier to solve numerically. To reduce errors of the spatial semidiscretization, we use Fourier collocation methods with $N = 2^{12}$ nodes in the domain $[-35, 35]$.

The results shown in Figure 6 confirm the high accuracy of the time discretizations. In all cases, using relaxation to conserve mass and energy increases the accuracy. This effect is particularly pronounced for the odd-order methods ARS3 (also known as ARS(4,4,3) of [8]) and KC5 (ARK5(4)8L[2]SA₂ of [46]). Moreover, this demonstrates that the new relaxation approach works robustly.

3.4 Error growth for multiple-soliton solutions

In [5] it was shown that, under certain assumptions and in the context of the KdV equation, numerical methods that conserve N invariants also exhibit linear error growth for N -soliton solutions. Here we test experimentally whether this holds for NLS and $N = 2$; we also investigate the behavior of the error for three solitons, which goes beyond any existing theory since we have only two numerically conserved quantities. We use the same setup as in [16], employing Fourier collocation methods with $N = 2^{10}$ nodes in the domain $[-35, 35]$ for the spatial semidiscretization and the fifth-order method of [46] for the time discretization.

The results shown in Figure 7 confirm the advantages of using relaxation to conserve mass and energy. In particular, the error grows quadratically in time for the baseline method and only linearly in time for the relaxed method. Remarkably, we see this behavior not only for the two-soliton case (in agreement with [5]) but even with three solitons.

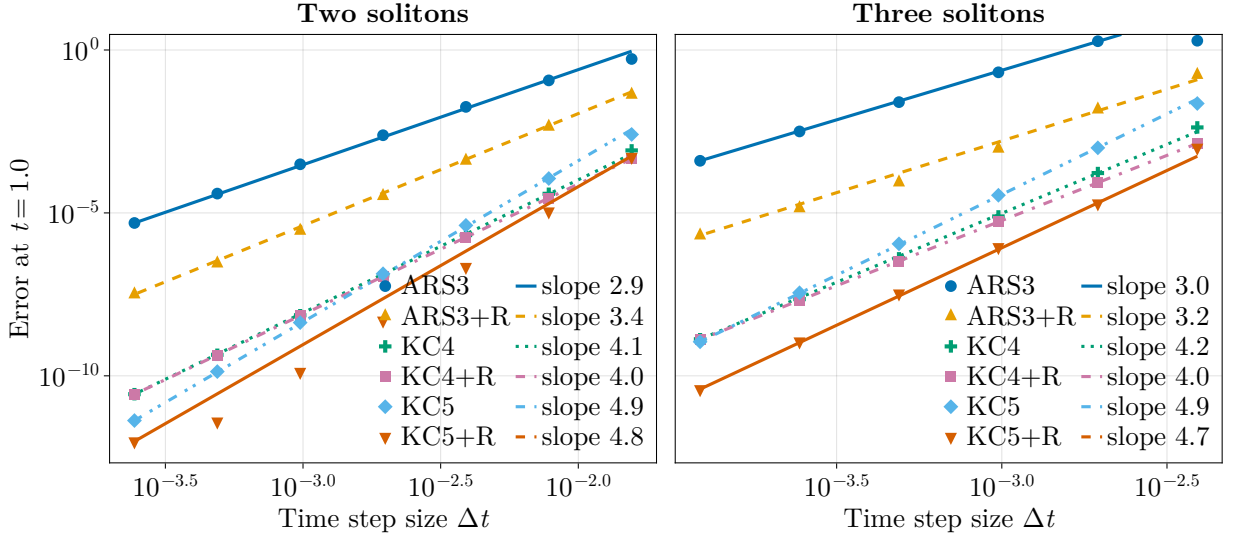


Figure 6: Temporal convergence study for the two- and three-soliton setups using Fourier collocation methods with $N = 2^{12}$ nodes in the domain $[-35, 35]$ in space. ARS3 is the third-order method of [8] and KC4/5 are the fourth/fifth-order methods of [46]. “+R” indicates relaxation to conserve mass and energy.

3.5 Error growth for a gray soliton

Next, we consider the defocusing case $\beta = -1$. Following [28], we consider the gray soliton expressed in terms of the hydrodynamic variables

$$\varrho = b_1 - \frac{b_1 - b_2}{\cosh^2\left(\sqrt{b_1 - b_2}(x/\sqrt{2} - ct)\right)}, \quad v = c - \frac{b_1\sqrt{b_2}}{\varrho}, \quad (3.18)$$

obtained from the Madelung transformation

$$u = \sqrt{\varrho} \exp(i\theta), \quad v = \theta_x. \quad (3.19)$$

As in [28, Section 5.1], we use the parameters $b_1 = 1$, $b_2 = 1.5$, and $c = 2$. The scaling factor $\sqrt{2}$ of x is chosen to compensate for the different choice of constants in the NLS equation in [28].

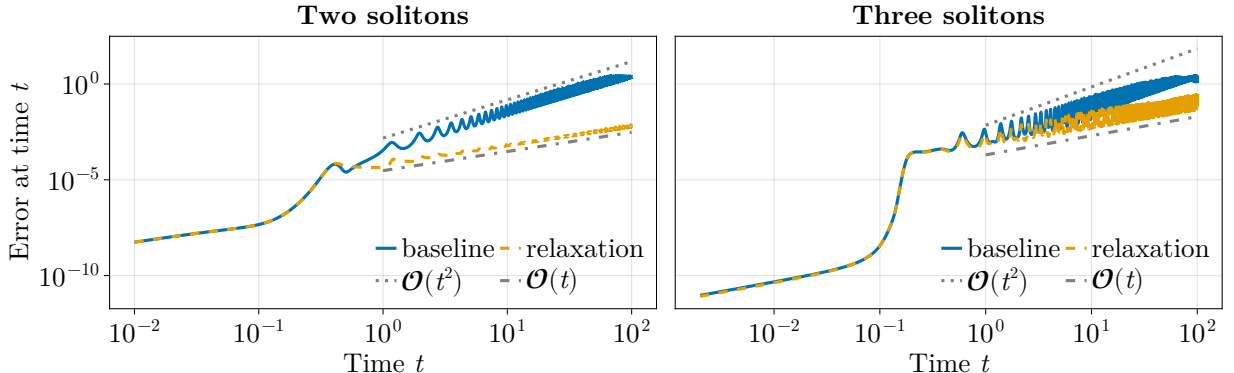


Figure 7: Error growth in time for the two- and three-soliton setups using Fourier collocation methods with $N = 2^{10}$ nodes in the domain $[-35, 35]$ in space and the fifth-order method of [46] with time step size $\Delta t = 10^{-2}$ (two solitons) and $\Delta t = 2 \times 10^{-3}$ (three solitons).

Since the gray soliton is given in terms of the hydrodynamic velocity v and we use the classical variable u , we compute θ by integrating v numerically using the adaptive Gauss-Kronrod quadrature implemented in QuadGK.jl [44]. We choose a periodic domain with left boundary -30 and compute the right boundary ≈ 33.9412 such that the initial condition is periodic using the root finding algorithm of [48] implemented in SimpleNonlinearSolve.jl [59].

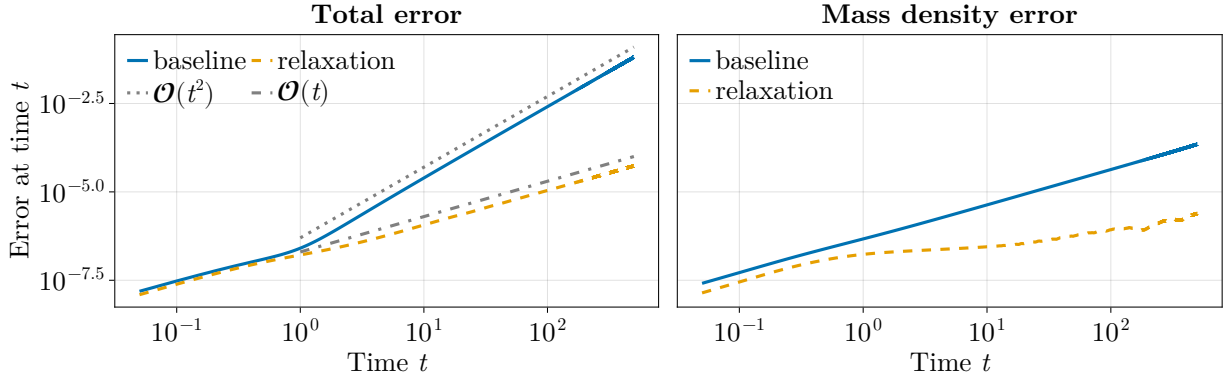


Figure 8: Error growth in time for the gray soliton setup using Fourier collocation methods with $N = 2^8$ nodes in space and the fifth-order method of [46] with time step size $\Delta t = 0.05$.

The results shown in Figure 8 confirm again the advantages of using relaxation to conserve mass and energy. In particular, the total error grows again quadratically in time for the baseline method and only linearly in time for the relaxed method. In contrast, the discrete L^2 error of the mass density $|u|^2 = v^2 + w^2$ grows only linearly in time, even without relaxation.

4 Performance comparison

Next, we compare the performance of our proposed approach to other methods from the literature. As described in [16, Section 5.2], the best performing methods from their comparison are the linearly implicit method of Besse et al. [12, 13] with uniform time step sizes (limited to second-order accuracy in time) with arbitrarily high-order finite differences in space and the multiple-relaxation method of Biswas and Ketcheson [16] with time step size control and a continuous finite element method in space (limited to second-order accuracy in space). In their comparison, these two methods perform similarly. Thus, we only compare our approach to the relaxation method of Besse et al. [12, 13].

We have implemented all methods with a reasonable amount of effort to ensure a fair comparison. For example, we have re-used the symbolic factorization of sparse matrices for the linearly implicit method of Besse et al.; please note that the system matrix changes in every time step for this method, so that we have to re-assemble and re-factor the system matrix quite often. Because of these measures (and using Julia instead of Python), our implementations are more efficient than the ones provided by [16] (roughly by a factor between three and 13 for the results reported in [16, Table 6]).

For the IMEX methods with quadratic-preserving relaxation, the system matrices do not depend on the numerical solution but only on the time step size; we store and re-use the sparse LU factorizations of these matrices. We only consider Fourier methods in space for IMEX methods, where we can solve the resulting linear systems efficiently using the fast Fourier transform. We do not use Fourier methods for the scheme of Besse et al., since they already noted that their method is not competitive in this case [13, p. 642] due to the structure of the linear systems.

Following [16], we consider the two- and three-soliton setups in the spatial domain $[-35, 35]$ and compute the discrete L^2 error at the final time $t = 2$. To avoid limiting the error artificially by the spatial discretization, we use eighth-order FDs and Fourier collocation schemes. We solve the

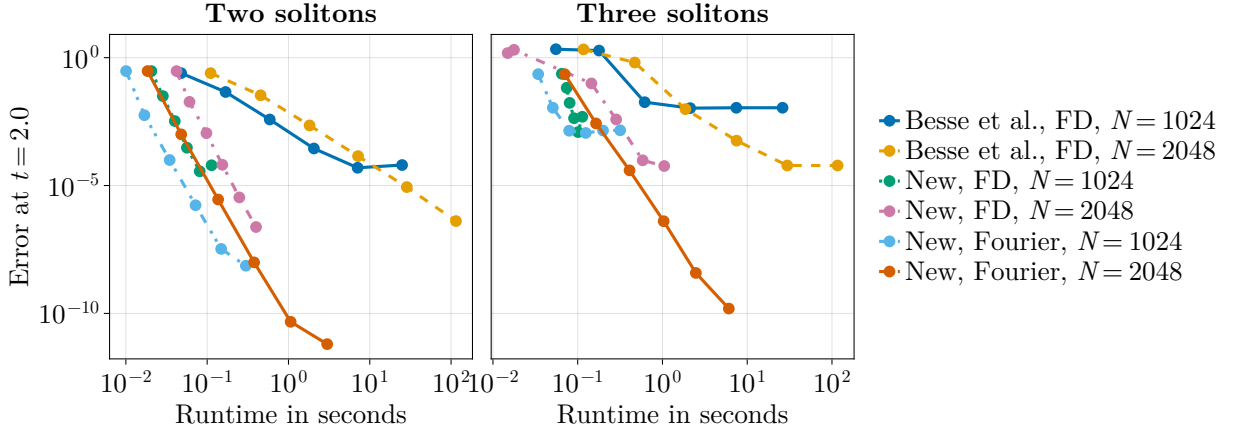


Figure 9: Error versus runtime for the two- and three-soliton setups using finite differences and Fourier collocation methods in the domain $[-35, 35]$. For our approach, we use the fifth-order method of [46] with quadratic-preserving relaxation to conserve mass and energy. For all methods, we used various uniform time step sizes.

problem three times on an Apple M4 MacBook Pro and take the minimum runtime to reduce the influence of noise.

The results visualized in Figure 9 demonstrate the advantage of our proposed methods combining arbitrarily high-order SBP operators in space with quadratic-preserving relaxation applied to high-order IMEX methods in time. For the same runtime, our approach achieves a significantly smaller error than the reference method. Moreover, the Fourier collocation method is more efficient than the FD method using sparse direct solvers.

Finally, we have run a rough comparison of our methods with those of [9]. We consider the one-soliton problem from Section 4 of that work, given by

$$u(x, t) = \operatorname{sech}(x + 4t) \exp(-i(2x + 3t)).$$

We solve the problem on the domain $x \in [-40, 40]$ for $0 \leq t \leq 1$ and measure the L^2 norm of the error at the final time. Using the same discretization considered in Figure 4.4(b) of that work the wall clock time for a run using $\Delta t = 1/512$ and 1024 points in space is approximately 90 seconds and results in an error of 1.26×10^{-6} . Meanwhile, using the method described here with the same number of time steps and spatial points, the wall clock time is less than 1/10 of one second and results in an error of 9.60×10^{-12} . We observe that the method here yields a much more accurate solution in a time that is approximately 4 orders of magnitude faster. The tests for both methods were performed on a workstation with two sockets of 20 dual-threaded Intel Xeon Gold 6230 CPUs running Ubuntu 22.04.

5 Hyperbolization of the nonlinear Schrödinger equation

Next, we consider the hyperbolization

$$\begin{aligned} iq_t^0 + q_x^1 &= -\beta|q^0|^2 q^0, \\ i\tau q_t^1 - q_x^0 &= -q^1 \end{aligned} \tag{5.1}$$

of the nonlinear Schrödinger equation (1.1) analyzed in [15]. Separating the real and imaginary parts as $q^0 = v + i\omega$ and $q^1 = v + i\omega$, we obtain

$$\begin{aligned} v_t &= -\omega_x - \beta(v^2 + w^2)w, \\ w_t &= v_x + \beta(v^2 + w^2)v, \\ \tau v_t &= w_x - \omega, \\ \tau \omega_t &= -v_x + \nu. \end{aligned} \tag{5.2}$$

This system has three nonlinear invariants approximating the mass, momentum, and energy of the NLS (1.1) (formally) for $\tau \rightarrow 0$ [15]. Mass-conserving semidiscretizations using periodic first-derivative SBP operators have been proposed in [15, Section 4]¹. Here, we generalize this approach to upwind SBP operators, avoiding issues with wide-stencil second-derivative operators in the FD framework. From the point of view of DG methods, this means we use LDG methods with alternating upwind fluxes instead of the Bassi-Rebay 1 (BR1) scheme. Concretely, we propose the semidiscretization

$$\begin{aligned} \partial_t \mathbf{v} &= -D_- \boldsymbol{\omega} - \beta(\mathbf{v}^2 + \mathbf{w}^2)\mathbf{w}, \\ \partial_t \mathbf{w} &= D_- \mathbf{v} + \beta(\mathbf{v}^2 + \mathbf{w}^2)\mathbf{v}, \\ \tau \partial_t \mathbf{v} &= D_+ \mathbf{w} - \boldsymbol{\omega}, \\ \tau \partial_t \boldsymbol{\omega} &= -D_+ \mathbf{v} + \mathbf{v}, \end{aligned} \tag{5.3}$$

where D_{\pm} are periodic upwind operators. The corresponding discrete total mass is

$$\begin{aligned} \mathcal{M} &= \mathbf{v}^T M \mathbf{v} + \mathbf{w}^T M \mathbf{w} + \tau \mathbf{v}^T M \mathbf{v} + \tau \boldsymbol{\omega}^T M \boldsymbol{\omega} \\ &\approx \int (v^2 + w^2 + \tau v^2 + \tau \omega^2) dx = \int (|q^0|^2 + \tau |q^1|^2) dx, \end{aligned} \tag{5.4}$$

and the discrete total energy is

$$\begin{aligned} \mathcal{E} &= 2\mathbf{v}^T M D_+ \mathbf{v} - \mathbf{v}^T M \mathbf{v} + 2\boldsymbol{\omega}^T M D_+ \mathbf{w} - \boldsymbol{\omega}^T M \boldsymbol{\omega} - \frac{\beta}{2} \mathbf{1}^T M (\mathbf{v}^2 + \mathbf{w}^2)^2 \\ &\approx \int \left(2v v_x - v^2 + 2\omega w_x - \omega^2 - \frac{\beta}{2} (v^2 + w^2)^2 \right) dx \\ &= \int \left(\overline{q^1} q_x^0 + q^1 \overline{q_x^0} - |q^1|^2 - \frac{\beta}{2} |q^0|^4 \right) dx. \end{aligned} \tag{5.5}$$

As $\tau \rightarrow 0$, we (formally) have $\mathbf{v} \rightarrow D_+ \mathbf{v}$ and $\boldsymbol{\omega} \rightarrow D_+ \boldsymbol{\omega}$ in (5.3), i.e., the semidiscretization (5.3) converges to the semidiscretization (2.11) of the nonlinear Schrödinger equation (1.1) with second-derivative SBP operator $D_2 = D_- D_+$.

Theorem 5.1. *The semidiscretization (5.3) conserves the discrete total mass (5.4) and the discrete total energy (5.5) for diagonal-norm upwind SBP operators.*

Proof. We compute

$$\begin{aligned} \frac{1}{2} \partial_t \mathcal{M} &= \mathbf{v}^T M \partial_t \mathbf{v} + \mathbf{w}^T M \partial_t \mathbf{w} + \tau \mathbf{v}^T M \partial_t \mathbf{v} + \tau \boldsymbol{\omega}^T M \partial_t \boldsymbol{\omega} \\ &= -\mathbf{v}^T M D_- \boldsymbol{\omega} - \beta \mathbf{v}^T M (\mathbf{v}^2 + \mathbf{w}^2) \mathbf{w} + \mathbf{w}^T M D_- \mathbf{v} + \beta \mathbf{w}^T M (\mathbf{v}^2 + \mathbf{w}^2) \mathbf{v} \\ &\quad + \mathbf{v}^T M D_+ \mathbf{w} - \mathbf{v}^T M \boldsymbol{\omega} - \boldsymbol{\omega}^T M D_+ \mathbf{v} + \boldsymbol{\omega}^T M \mathbf{v} \\ &= -\mathbf{v}^T M D_- \boldsymbol{\omega} - \boldsymbol{\omega}^T M D_+ \mathbf{v} + \mathbf{w}^T M D_- \mathbf{v} + \mathbf{v}^T M D_+ \mathbf{w} = 0, \end{aligned} \tag{5.6}$$

¹They required skew-Hermitian derivative operators in periodic domains, i.e., SBP operators with mass matrices proportional to the identity matrix such as classical central finite differences or Fourier collocation methods.

where we used the periodic upwind SBP property and that the mass matrix M is diagonal. Next, we compute

$$\begin{aligned}
& \frac{1}{2} \partial_t \mathcal{E} \\
&= \mathbf{v}^T M D_+ \partial_t \mathbf{v} + \mathbf{v}^T D_+^T M \partial_t \mathbf{v} - \mathbf{v}^T M \partial_t \mathbf{v} + \boldsymbol{\omega}^T M D_+ \partial_t \mathbf{w} + \mathbf{w}^T D_+^T M \partial_t \boldsymbol{\omega} - \boldsymbol{\omega}^T M \partial_t \boldsymbol{\omega} \\
&\quad - \beta \mathbf{1}^T M (\mathbf{v}^2 + \mathbf{w}^2) \mathbf{v} \partial_t \mathbf{v} - \beta \mathbf{1}^T M (\mathbf{v}^2 + \mathbf{w}^2) \mathbf{w} \partial_t \mathbf{w} \\
&= -\mathbf{v}^T M D_+ D_- \boldsymbol{\omega} - \beta \mathbf{v}^T M D_+ (\mathbf{v}^2 + \mathbf{w}^2) \mathbf{w} + \tau^{-1} \mathbf{v}^T D_+^T M D_+ \mathbf{w} - \tau^{-1} \mathbf{v}^T D_+^T M \boldsymbol{\omega} \\
&\quad - \tau^{-1} \mathbf{v}^T M D_+ \mathbf{w} + \tau^{-1} \mathbf{v}^T M \boldsymbol{\omega} - \boldsymbol{\omega}^T M D_+ D_- \mathbf{v} + \beta \boldsymbol{\omega}^T M D_+ (\mathbf{v}^2 + \mathbf{w}^2) \mathbf{v} \\
&\quad - \tau^{-1} \mathbf{w}^T D_+^T M D_+ \mathbf{v} + \tau^{-1} \mathbf{w}^T D_+^T M \boldsymbol{\omega} + \tau^{-1} \boldsymbol{\omega}^T M D_+ \mathbf{v} - \tau^{-1} \boldsymbol{\omega}^T M \mathbf{v} \\
&\quad + \beta \mathbf{1}^T M (\mathbf{v}^2 + \mathbf{w}^2) \mathbf{v} D_- \boldsymbol{\omega} + \beta^2 \mathbf{1}^T M (\mathbf{v}^2 + \mathbf{w}^2)^2 \mathbf{v} \mathbf{w} \\
&\quad - \beta \mathbf{1}^T M (\mathbf{v}^2 + \mathbf{w}^2) \mathbf{w} D_- \mathbf{v} - \beta^2 \mathbf{1}^T M (\mathbf{v}^2 + \mathbf{w}^2)^2 \mathbf{v} \mathbf{w} \\
&= -\mathbf{v}^T M D_+ D_- \boldsymbol{\omega} - \beta \mathbf{v}^T M D_+ (\mathbf{v}^2 + \mathbf{w}^2) \mathbf{w} - \boldsymbol{\omega}^T M D_+ D_- \mathbf{v} + \beta \boldsymbol{\omega}^T M D_+ (\mathbf{v}^2 + \mathbf{w}^2) \mathbf{v} \\
&\quad + \beta \mathbf{1}^T M (\mathbf{v}^2 + \mathbf{w}^2) \mathbf{v} D_- \boldsymbol{\omega} - \beta \mathbf{1}^T M (\mathbf{v}^2 + \mathbf{w}^2) \mathbf{w} D_- \mathbf{v} = 0,
\end{aligned} \tag{5.7}$$

where we canceled terms in the second step and used the periodic upwind SBP property as well as the fact that the mass matrix M is diagonal in the last step. \square

The semidiscrete hyperbolization (5.3) cannot recover all semidiscretizations discussed above for the standard nonlinear Schrödinger equation (1.1) in the limit $\tau \rightarrow 0$. In particular, it can only recover second-derivative operators that can be factored as product of first-derivative upwind operators. This excludes, for example, Fourier collocation methods with an even number of nodes (unless the second-derivative operator uses the “wrong” treatment of the highest frequency mode [43]) or narrow-stencil FD operators with order of accuracy four or higher. However, LDG methods with alternating upwind fluxes or second-derivative FD operators using a product of two alternating upwind FD operators can be recovered in the limit $\tau \rightarrow 0$.

5.1 Mass projection

Since the mass (5.5) of the hyperbolized NLS scales the approximation variables $\mathbf{v}, \boldsymbol{\omega}$ by τ , we have to consider a projection onto an ellipsoid instead of a sphere. Since the exact orthogonal projection does not have a simple closed-form solution², we use a simplified projection algorithm as in [36, Section IV.4] instead: we project along the direction orthogonal to the constant-mass ellipsoid based on the current solution. Given values $\mathbf{v}, \mathbf{w}, \boldsymbol{\nu}$, and $\boldsymbol{\omega}$, the simplified projection scales \mathbf{v}, \mathbf{w} by α_1 and $\boldsymbol{\nu}, \boldsymbol{\omega}$ by α_2 , where

$$\begin{aligned}
\alpha_1 &= \frac{p(\tau-1)\tau^2 + \sqrt{-pq(\tau-1)^2\tau + c(q+p\tau^3)}}{q+p\tau^3}, \\
\alpha_2 &= \frac{q(1-\tau) + \tau\sqrt{-p^2q^2(\tau-1)^2\tau + c(q^2+p^2\tau^3)}}{q^2+p^2\tau^3},
\end{aligned} \tag{5.8}$$

c is the desired value of the mass (5.5), and

$$q = \|\mathbf{v}\|_M^2 + \|\mathbf{w}\|_M^2, \quad p = \|\boldsymbol{\nu}\|_M^2 + \|\boldsymbol{\omega}\|_M^2. \tag{5.9}$$

²We have to find a root of a quartic polynomial, for which no simple closed-form solution exists.

5.2 Numerical results

The semidiscretization (5.3) of the hyperbolized NLS behaves as expected. The asymptotic-preserving properties can be analyzed as demonstrated in [15]. Here, we only present selected numerical results demonstrating fully-discrete conservation of the total mass (5.4) and the total energy (5.5).

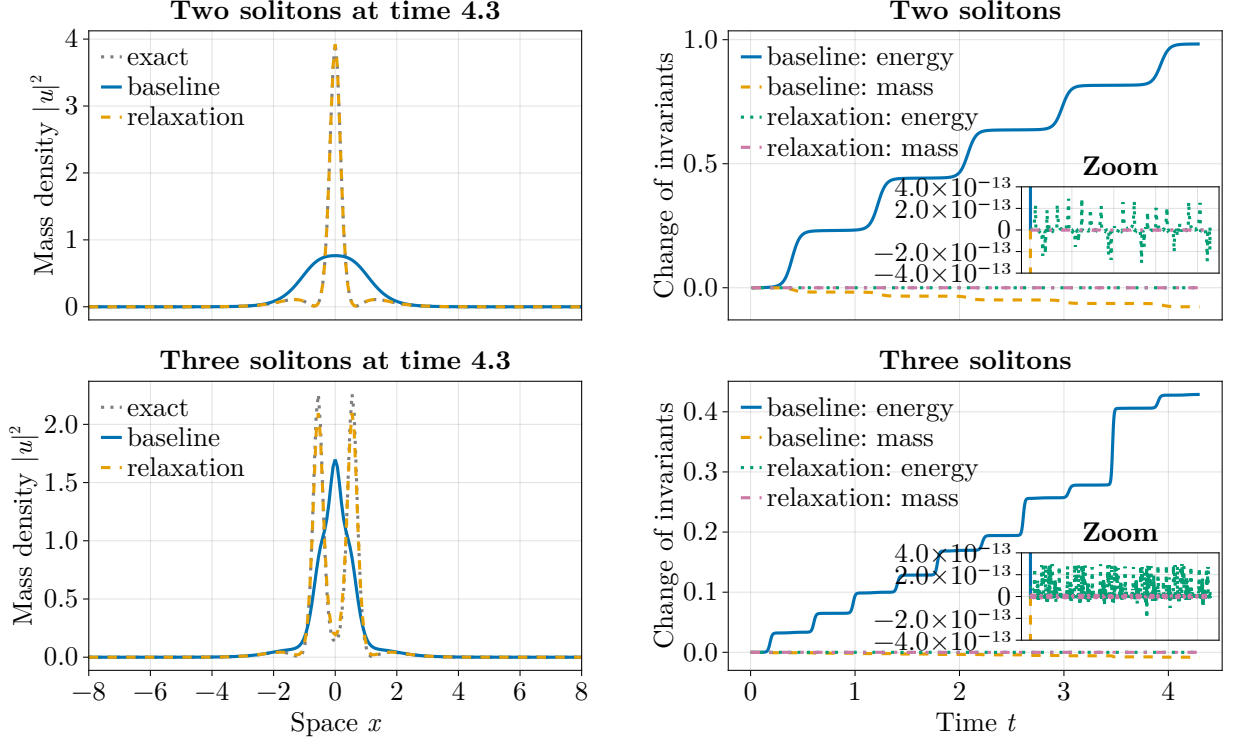


Figure 10: Numerical results obtained for the two- ($\Delta t = 10^{-2}$) and three-soliton ($\Delta t = 10^{-3}$) setups for the hyperbolized nonlinear Schrödinger equation with $\tau = 10^{-4}$ using sixth-order upwind FD SBP operators with $N = 2^{10}$ nodes in the domain $[-35, 35]$ in space and the third-order method of [8] in time.

We discretize the domain $[-35, 35]$ with sixth-order upwind FD SBP operators with $N = 2^{10}$ nodes. We use well-prepared initial data for the hyperbolization, i.e., we use the initial values $\mathbf{v}^0 = D_+ \mathbf{v}^0$ and $\boldsymbol{\omega}^0 = D_+ \boldsymbol{\omega}^0$. Results with and without relaxation for are shown in Figure 10. As expected, the results are similar to the ones obtained with the baseline nonlinear Schrödinger equation, see Figure 5. We clearly observe a significant improvement of the numerical solutions by conserving the total mass and energy discretely using quadratic-preserving relaxation.

6 Summary and discussion

In this work we have shed new light on the conservation properties of existing schemes in addition to proposing new efficient conservative schemes for the NLS equation and its hyperbolic approximation. Our analysis makes it clear that using Fourier spectral differentiation in space yields a semidiscrete scheme that conserves discrete analogs of both mass and energy, as do all methods that use a broad class of SBP operators.

Our new quadratic-preserving relaxation method extends these conservation properties to the fully-discrete setting, in a manner that we have shown to be more robust and computationally efficient compared to multiple relaxation. As our new approach is focused on the time discretization, it can immediately be brought to bear on multidimensional applications of NLS. The quadratic-

preserving relaxation technique can also be applied to other systems that possess both quadratic and non-quadratic nonlinear conserved functionals. Furthermore, it suggests a natural extension in order to conserve more than two conserved quantities. The analysis and application of these generalizations is the subject of ongoing work.

Acknowledgments

HR was supported by the Deutsche Forschungsgemeinschaft (DFG, German Research Foundation, project numbers 513301895 and 528753982 as well as within the DFG priority program SPP 2410 with project number 526031774). DK was supported by funding from King Abdullah University of Science and Technology.

We thank Ángel Durán for hosting us in Valladolid during the week September 15–19 2025, where this project was initiated.

References

- [1] R. Abgrall, E. L. Mélédo, P. Öffner, and D. Torlo. “Relaxation Deferred Correction Methods and their Applications to Residual Distribution Schemes.” In: *The SMAI Journal of Computational Mathematics* 8 (2022), pp. 125–160. doi: [10.5802/smai-jcm.82](https://doi.org/10.5802/smai-jcm.82). arXiv: [2106.05005](https://arxiv.org/abs/2106.05005) [math.NA].
- [2] R. Abgrall, J. Nordström, P. Öffner, and S. Tokareva. “Analysis of the SBP-SAT Stabilization for Finite Element Methods Part I: Linear problems.” In: *Journal of Scientific Computing* 85.2 (2020), pp. 1–29. doi: [10.1007/s10915-020-01349-z](https://doi.org/10.1007/s10915-020-01349-z). arXiv: [1912.08108](https://arxiv.org/abs/1912.08108) [math.NA].
- [3] G. Akrivis, B. Li, R. Tang, and H. Zhang. “High-order mass-, energy-and momentum-conserving methods for the nonlinear Schrödinger equation.” In: *Journal of Computational Physics* 532 (2025), p. 113974. doi: [10.1016/j.jcp.2025.113974](https://doi.org/10.1016/j.jcp.2025.113974).
- [4] G. D. Akrivis, V. A. Dougalis, and O. A. Karakashian. “On fully discrete Galerkin methods of second-order temporal accuracy for the nonlinear Schrödinger equation.” In: *Numerische Mathematik* 59.1 (1991), pp. 31–53. doi: [10.1007/BF01385769](https://doi.org/10.1007/BF01385769).
- [5] J. Álvarez and A. Durán. “Error propagation when approximating multi-solitons: The KdV equation as a case study.” In: *Applied Mathematics and Computation* 217.4 (2010), pp. 1522–1539.
- [6] P. R. Amestoy, T. A. Davis, and I. S. Duff. “Algorithm 837: AMD, an approximate minimum degree ordering algorithm.” In: *ACM Transactions on Mathematical Software (TOMS)* 30.3 (2004), pp. 381–388. doi: [10.1145/1024074.1024081](https://doi.org/10.1145/1024074.1024081).
- [7] X. Antoine, C. Besse, and V. Rispoli. “High-order IMEX-spectral schemes for computing the dynamics of systems of nonlinear Schrödinger/Gross–Pitaevskii equations.” In: *Journal of Computational Physics* 327 (2016), pp. 252–269.
- [8] U. M. Ascher, S. J. Ruuth, and R. J. Spiteri. “Implicit-explicit Runge-Kutta methods for time-dependent partial differential equations.” In: *Applied Numerical Mathematics* 25.2-3 (1997), pp. 151–167. doi: [10.1016/S0168-9274\(97\)00056-1](https://doi.org/10.1016/S0168-9274(97)00056-1).
- [9] G. Bai, J. Hu, and B. Li. “High-order mass-and energy-conserving methods for the nonlinear Schrödinger equation.” In: *SIAM Journal on Scientific Computing* 46.2 (2024), A1026–A1046. doi: [10.1137/22M152178X](https://doi.org/10.1137/22M152178X).
- [10] W. Bao, S. Jin, and P. A. Markowich. “On time-splitting spectral approximations for the Schrödinger equation in the semiclassical regime.” In: *Journal of Computational Physics* 175.2 (2002), pp. 487–524. doi: [10.1006/jcph.2001.6956](https://doi.org/10.1006/jcph.2001.6956).

- [11] W. Barsukow, C. Klingenberg, L. Lechner, J. Nordström, S. Ortlob, and H. Ranocha. *Stability of the Active Flux Method in the Framework of Summation-by-Parts Operators*. July 2025. arXiv: 2507.11068 [math.NA].
- [12] C. Besse. “A relaxation scheme for the nonlinear Schrödinger equation.” In: *SIAM Journal on Numerical Analysis* 42.3 (2004), pp. 934–952. doi: 10.1137/S0036142901396521.
- [13] C. Besse, S. Descombes, G. Dujardin, and I. Lacroix-Violet. “Energy-preserving methods for nonlinear Schrödinger equations.” In: *IMA Journal of Numerical Analysis* 41.1 (2021), pp. 618–653. doi: 10.1093/imanum/drz067.
- [14] J. Bezanson, A. Edelman, S. Karpinski, and V. B. Shah. “Julia: A Fresh Approach to Numerical Computing.” In: *SIAM Review* 59.1 (2017), pp. 65–98. doi: 10.1137/141000671. arXiv: 1411.1607 [cs.MS].
- [15] A. Biswas, L. S. Busaleh, D. I. Ketcheson, C. Muñoz-Moncayo, and M. Rajvanshi. *A Hyperbolic Approximation of the Nonlinear Schrödinger Equation*. 2025. arXiv: 2505.21424 [math.AP].
- [16] A. Biswas and D. I. Ketcheson. “Accurate Solution of the Nonlinear Schrödinger Equation via Conservative Multiple-Relaxation ImEx Methods.” In: *SIAM Journal of Scientific Computing* 46.6 (2024), A3827–A3848. doi: 10.1137/23M1598118. arXiv: 2309.02324 [math.NA].
- [17] A. Biswas and D. I. Ketcheson. “Multiple-relaxation Runge Kutta methods for conservative dynamical systems.” In: *Journal of Scientific Computing* 97.1 (2023), p. 4. doi: 10.1007/s10915-023-02312-4.
- [18] M. Calvo, M. Laburta, J. I. Montijano, and L. Rández. “Projection methods preserving Lyapunov functions.” In: *BIT Numerical Mathematics* 50.2 (2010), pp. 223–241. doi: 10.1007/s10543-010-0259-3.
- [19] W. Cao, D. Li, and Z. Zhang. “Optimal superconvergence of energy conserving local discontinuous Galerkin methods for wave equations.” In: *Communications in Computational Physics* 21.1 (2017), pp. 211–236. doi: 10.4208/cicp.120715.100516a.
- [20] M. H. Carpenter, T. C. Fisher, E. J. Nielsen, and S. H. Frankel. “Entropy Stable Spectral Collocation Schemes for the Navier-Stokes Equations: Discontinuous Interfaces.” In: *SIAM Journal on Scientific Computing* 36.5 (2014), B835–B867. doi: 10.1137/130932193.
- [21] M. H. Carpenter, D. Gottlieb, and S. Abarbanel. “Time-Stable Boundary Conditions for Finite-Difference Schemes Solving Hyperbolic Systems: Methodology and Application to High-Order Compact Schemes.” In: *Journal of Computational Physics* 111.2 (1994), pp. 220–236. doi: 10.1006/jcph.1994.1057.
- [22] J. Cui, Z. Xu, Y. Wang, and C. Jiang. “Mass-and energy-preserving exponential Runge-Kutta methods for the nonlinear Schrödinger equation.” In: *Applied Mathematics Letters* 112 (2021), p. 106770. doi: 10.1016/j.aml.2020.106770.
- [23] S. Danisch and J. Krumbiegel. “Makie.jl: Flexible high-performance data visualization for Julia.” In: *Journal of Open Source Software* 6.65 (2021), p. 3349. doi: 10.21105/joss.03349.
- [24] T. A. Davis. “Algorithm 832: UMFPACK V4.3—an unsymmetric-pattern multifrontal method.” In: *ACM Transactions on Mathematical Software (TOMS)* 30.2 (2004), pp. 196–199. doi: 10.1145/992200.992206.
- [25] T. A. Davis, J. R. Gilbert, S. I. Larimore, and E. G. Ng. “Algorithm 836: COLAMD, a column approximate minimum degree ordering algorithm.” In: *ACM Transactions on Mathematical Software (TOMS)* 30.3 (2004), pp. 377–380. doi: 10.1145/1024074.1024080.
- [26] K. Dekker and J. G. Verwer. *Stability of Runge-Kutta methods for stiff nonlinear differential equations*. Vol. 2. CWI Monographs. Amsterdam: North-Holland, 1984.
- [27] M. Delfour, M. Fortin, and G Payr. “Finite-difference solutions of a non-linear Schrödinger equation.” In: *Journal of computational physics* 44.2 (1981), pp. 277–288. doi: 10.1016/0021-9991(81)90052-8.

- [28] F. Dhaouadi, N. Favrie, and S. Gavrilyuk. “Extended Lagrangian approach for the defocusing nonlinear Schrödinger equation.” In: *Studies in Applied Mathematics* 142.3 (2019), pp. 336–358. doi: [10.1111/sapm.12238](https://doi.org/10.1111/sapm.12238).
- [29] D. Doehring, H. Ranocha, and M. Torrilhon. *Paired Explicit Relaxation Runge-Kutta Methods: Entropy-Conservative and Entropy-Stable High-Order Optimized Multirate Time Integration*. July 2025. arXiv: [2507.04991](https://arxiv.org/abs/2507.04991) [math.NA].
- [30] J. Douglas Jr and T. Dupont. “Superconvergence for Galerkin methods for the two point boundary problem via local projections.” In: *Numerische Mathematik* 21.3 (1973), pp. 270–278. doi: [10.1007/BF01436631](https://doi.org/10.1007/BF01436631).
- [31] T. Eymann and P. Roe. “Active flux schemes.” In: *49th AIAA Aerospace Sciences Meeting including the New Horizons Forum and Aerospace Exposition*. 2011, p. 382. doi: [10.2514/6.2011-382](https://doi.org/10.2514/6.2011-382).
- [32] D. C. D. R. Fernández, J. E. Hicken, and D. W. Zingg. “Review of summation-by-parts operators with simultaneous approximation terms for the numerical solution of partial differential equations.” In: *Computers & Fluids* 95 (2014), pp. 171–196. doi: [10.1016/j.compfluid.2014.02.016](https://doi.org/10.1016/j.compfluid.2014.02.016).
- [33] M. Frigo and S. G. Johnson. “The design and implementation of FFTW3.” In: *Proceedings of the IEEE* 93.2 (2005), pp. 216–231. doi: [10.1109/JPROC.2004.840301](https://doi.org/10.1109/JPROC.2004.840301).
- [34] G. J. Gassner. “A Skew-Symmetric Discontinuous Galerkin Spectral Element Discretization and Its Relation to SBP-SAT Finite Difference Methods.” In: *SIAM Journal on Scientific Computing* 35.3 (2013), A1233–A1253. doi: [10.1137/120890144](https://doi.org/10.1137/120890144).
- [35] A. Gurevich and A. Krylov. “Dissipationless shock waves in media with positive dispersion.” In: *Zh. Eksp. Teor. Fiz.* 92 (1987), p. 1684.
- [36] E. Hairer, C. Lubich, and G. Wanner. *Geometric Numerical Integration: Structure-Preserving Algorithms for Ordinary Differential Equations*. Vol. 31. Springer Series in Computational Mathematics. Berlin Heidelberg: Springer-Verlag, 2006. doi: [10.1007/3-540-30666-8](https://doi.org/10.1007/3-540-30666-8).
- [37] P. Henning and D. Peterseim. “Crank-Nicolson Galerkin approximations to nonlinear Schrödinger equations with rough potentials.” In: *Mathematical Models and Methods in Applied Sciences* 27.11 (2017), pp. 2147–2184. doi: [10.1142/S0218202517500415](https://doi.org/10.1142/S0218202517500415).
- [38] B. M. Herbst, J. L. Morris, and A. R. Mitchell. “Numerical experience with the nonlinear Schrödinger equation.” In: *Journal of Computational Physics* 60.2 (1985), pp. 282–305. doi: [10.1016/0021-9991\(85\)90008-7](https://doi.org/10.1016/0021-9991(85)90008-7).
- [39] J. Hicken, G. Yan, and S. Kaur. *Constructing stable, high-order finite-difference operators on point clouds over complex geometries*. Sept. 2024. arXiv: [2409.00809](https://arxiv.org/abs/2409.00809) [math.NA].
- [40] J. E. Hicken. “Entropy-stable, high-order summation-by-parts discretizations without interface penalties.” In: *Journal of Scientific Computing* 82.2 (2020), p. 50. doi: [10.1007/s10915-020-01154-8](https://doi.org/10.1007/s10915-020-01154-8).
- [41] J. E. Hicken, D. C. D. R. Fernández, and D. W. Zingg. “Multidimensional Summation-By-Parts Operators: General Theory and Application to Simplex Elements.” In: *SIAM Journal on Scientific Computing* 38.4 (2016), A1935–A1958. doi: [10.1137/15M1038360](https://doi.org/10.1137/15M1038360).
- [42] H. T. Huynh. “A Flux Reconstruction Approach to High-Order Schemes Including Discontinuous Galerkin Methods.” In: *18th AIAA Computational Fluid Dynamics Conference*. American Institute of Aeronautics and Astronautics. 2007. doi: [10.2514/6.2007-4079](https://doi.org/10.2514/6.2007-4079).
- [43] S. G. Johnson. *Notes on FFT-based differentiation*. <https://math.mit.edu/~stevenj/fft-deriv.pdf>. 2011.
- [44] S. G. Johnson. *QuadGK.jl: Gauss–Kronrod integration in Julia*. <https://github.com/JuliaMath/QuadGK.jl>. 2013.

- [45] S. Kang and E. M. Constantinescu. "Entropy-Preserving and Entropy-Stable Relaxation IMEX and Multirate Time-Stepping Methods." In: *Journal of Scientific Computing* 93 (2022), p. 23. doi: [10.1007/s10915-022-01982-w](https://doi.org/10.1007/s10915-022-01982-w). arXiv: [2108.08908](https://arxiv.org/abs/2108.08908) [math.NA].
- [46] C. A. Kennedy and M. H. Carpenter. "Higher-order additive Runge-Kutta schemes for ordinary differential equations." In: *Applied Numerical Mathematics* 136 (2019), pp. 183–205. doi: [10.1016/j.apnum.2018.10.007](https://doi.org/10.1016/j.apnum.2018.10.007).
- [47] D. I. Ketcheson. "Relaxation Runge-Kutta Methods: Conservation and Stability for Inner-Product Norms." In: *SIAM Journal on Numerical Analysis* 57.6 (2019), pp. 2850–2870. doi: [10.1137/19M1263662](https://doi.org/10.1137/19M1263662). arXiv: [1905.09847](https://arxiv.org/abs/1905.09847) [math.NA].
- [48] J. Klement. "On Using Quasi-Newton Algorithms of the Broyden Class for Model-to-test Correlation." In: *Journal of Aerospace Technology and Management* 6.4 (2014), pp. 407–414.
- [49] H.-O. Kreiss and G. Scherer. "Finite Element and Finite Difference Methods for Hyperbolic Partial Differential Equations." In: *Mathematical Aspects of Finite Elements in Partial Differential Equations*. Ed. by C. de Boor. New York: Academic Press, 1974, pp. 195–212.
- [50] J. Lampert and H. Ranocha. *Structure-Preserving Numerical Methods for Two Nonlinear Systems of Dispersive Wave Equations*. Feb. 2024. arXiv: [2402.16669](https://arxiv.org/abs/2402.16669) [math.NA].
- [51] T. Leibner and M. Ohlberger. "A new entropy-variable-based discretization method for minimum entropy moment approximations of linear kinetic equations." In: *ESAIM: Mathematical Modelling and Numerical Analysis* 55.6 (2021), pp. 2567–2608. doi: [10.1051/m2an/2021065](https://doi.org/10.1051/m2an/2021065).
- [52] D. Li and X. Li. "Relaxation Exponential Rosenbrock-Type Methods for Oscillatory Hamiltonian Systems." In: *SIAM Journal on Scientific Computing* 45.6 (2023), A2886–A2911. doi: [10.1137/22M1511345](https://doi.org/10.1137/22M1511345).
- [53] D. Li, X. Li, and Z. Zhang. "Implicit-explicit relaxation Runge-Kutta methods: construction, analysis and applications to PDEs." In: *Mathematics of Computation* (2022). doi: [10.1090/mcom/3766](https://doi.org/10.1090/mcom/3766).
- [54] H. Li, X. Li, K. Schratz, and B. Wang. *Time-Relaxation Structure-Preserving Explicit Low-Regularity Integrators for the Nonlinear Schrödinger Equation*. 2025. arXiv: [2510.02963](https://arxiv.org/abs/2510.02963) [math.NA].
- [55] K. Mattsson. "Diagonal-norm upwind SBP operators." In: *Journal of Computational Physics* 335 (2017), pp. 283–310. doi: [10.1016/j.jcp.2017.01.042](https://doi.org/10.1016/j.jcp.2017.01.042).
- [56] K. Mattsson and J. Nordström. "Summation by parts operators for finite difference approximations of second derivatives." In: *Journal of Computational Physics* 199.2 (2004), pp. 503–540. doi: [10.1016/j.jcp.2004.03.001](https://doi.org/10.1016/j.jcp.2004.03.001).
- [57] D. Mitsotakis, H. Ranocha, D. I. Ketcheson, and E. Süli. "A conservative fully-discrete numerical method for the regularized shallow water wave equations." In: *SIAM Journal on Scientific Computing* 42 (2 Apr. 2021), B508–B537. doi: [10.1137/20M1364606](https://doi.org/10.1137/20M1364606). arXiv: [2009.09641](https://arxiv.org/abs/2009.09641) [math.NA].
- [58] J. Nordström and M. Björck. "Finite volume approximations and strict stability for hyperbolic problems." In: *Applied Numerical Mathematics* 38.3 (2001), pp. 237–255. doi: [10.1016/S0168-9274\(01\)00027-7](https://doi.org/10.1016/S0168-9274(01)00027-7).
- [59] A. Pal, F. Holtorf, A. Larsson, T. Loman, Utkarsh, F. Schäfer, Q. Qu, A. Edelman, and C. Rackauckas. "NonlinearSolve.jl: High-Performance and Robust Solvers for Systems of Nonlinear Equations in Julia." In: (2024). doi: [10.48550/arXiv.2403.16341](https://doi.org/10.48550/arXiv.2403.16341). arXiv: [2403.16341](https://arxiv.org/abs/2403.16341) [math.NA].
- [60] H. Ranocha. "SummationByPartsOperators.jl: A Julia library of provably stable semidiscretization techniques with mimetic properties." In: *Journal of Open Source Software* 6.64 (Aug. 2021), p. 3454. doi: [10.21105/joss.03454](https://doi.org/10.21105/joss.03454). URL: <https://github.com/ranocha/SummationByPartsOperators.jl>.

- [61] H. Ranocha, L. Dalcin, and M. Parsani. “Fully-Discrete Explicit Locally Entropy-Stable Schemes for the Compressible Euler and Navier-Stokes Equations.” In: *Computers and Mathematics with Applications* 80.5 (July 2020), pp. 1343–1359. doi: [10.1016/j.camwa.2020.06.016](https://doi.org/10.1016/j.camwa.2020.06.016). arXiv: [2003.08831](https://arxiv.org/abs/2003.08831) [math.NA].
- [62] H. Ranocha and D. I. Ketcheson. “Relaxation Runge-Kutta Methods for Hamiltonian Problems.” In: *Journal of Scientific Computing* 84.1 (July 2020). doi: [10.1007/s10915-020-01277-y](https://doi.org/10.1007/s10915-020-01277-y). arXiv: [2001.04826](https://arxiv.org/abs/2001.04826) [math.NA].
- [63] H. Ranocha and D. I. Ketcheson. *Reproducibility repository for "High-order mass- and energy-conserving methods for the nonlinear Schrödinger equation and its hyperbolization"*. https://github.com/ranocha/2025_nls. 2025. doi: [10.5281/zenodo.17361026](https://doi.org/10.5281/zenodo.17361026).
- [64] H. Ranocha, L. Lóczki, and D. I. Ketcheson. “General Relaxation Methods for Initial-Value Problems with Application to Multistep Schemes.” In: *Numerische Mathematik* 146 (Oct. 2020), pp. 875–906. doi: [10.1007/s00211-020-01158-4](https://doi.org/10.1007/s00211-020-01158-4). arXiv: [2003.03012](https://arxiv.org/abs/2003.03012) [math.NA].
- [65] H. Ranocha, D. Mitsotakis, and D. I. Ketcheson. “A Broad Class of Conservative Numerical Methods for Dispersive Wave Equations.” In: *Communications in Computational Physics* 29.4 (Feb. 2021), pp. 979–1029. doi: [10.4208/cicp.OA-2020-0119](https://doi.org/10.4208/cicp.OA-2020-0119). arXiv: [2006.14802](https://arxiv.org/abs/2006.14802) [math.NA].
- [66] H. Ranocha, P. Öffner, and T. Sonar. “Summation-by-parts operators for correction procedure via reconstruction.” In: *Journal of Computational Physics* 311 (Apr. 2016), pp. 299–328. doi: [10.1016/j.jcp.2016.02.009](https://doi.org/10.1016/j.jcp.2016.02.009). arXiv: [1511.02052](https://arxiv.org/abs/1511.02052) [math.NA].
- [67] H. Ranocha and M. Ricchiuto. “Structure-preserving approximations of the Serre-Green-Naghdi equations in standard and hyperbolic form.” In: *Numerical Methods for Partial Differential Equations* 41.4 (June 2025), e70016. doi: [10.1002/num.70016](https://doi.org/10.1002/num.70016). arXiv: [2408.02665](https://arxiv.org/abs/2408.02665) [math.NA].
- [68] H. Ranocha, M. Sayyari, L. Dalcin, M. Parsani, and D. I. Ketcheson. “Relaxation Runge-Kutta Methods: Fully-Discrete Explicit Entropy-Stable Schemes for the Compressible Euler and Navier-Stokes Equations.” In: *SIAM Journal on Scientific Computing* 42.2 (Mar. 2020), A612–A638. doi: [10.1137/19M1263480](https://doi.org/10.1137/19M1263480). arXiv: [1905.09129](https://arxiv.org/abs/1905.09129) [math.NA].
- [69] H. Ranocha and J. Schütz. “Multiderivative time integration methods preserving nonlinear functionals via relaxation.” In: *Communications in Applied Mathematics and Computational Science* 19 (1 June 2024), pp. 27–56. doi: [10.2140/camcos.2024.19.27](https://doi.org/10.2140/camcos.2024.19.27). arXiv: [2311.03883](https://arxiv.org/abs/2311.03883) [math.NA].
- [70] H. Ranocha, J. Schütz, and E. Theodosiou. “Functional-preserving predictor-corrector multiderivative schemes.” In: *Proceedings in Applied Mathematics and Mechanics* (Sept. 2023). doi: [10.1002/pamm.202300025](https://doi.org/10.1002/pamm.202300025). arXiv: [2308.04876](https://arxiv.org/abs/2308.04876) [math.NA].
- [71] J. M. Sanz-Serna. “An explicit finite-difference scheme with exact conservation properties.” In: *Journal of Computational Physics* 47.2 (1982), pp. 199–210. doi: [10.1016/0021-9991\(82\)90074-2](https://doi.org/10.1016/0021-9991(82)90074-2).
- [72] J. M. Sanz-Serna. “Methods for the numerical solution of the nonlinear Schrödinger equation.” In: *Mathematics of Computation* 43.167 (1984), pp. 21–27. doi: [10.1090/S0025-5718-1984-0744922-X](https://doi.org/10.1090/S0025-5718-1984-0744922-X).
- [73] J. Sanz-Serna and V. Manoranjan. “A method for the integration in time of certain partial differential equations.” In: *Journal of Computational Physics* 52.2 (1983), pp. 273–289.
- [74] B. Strand. “Summation by Parts for Finite Difference Approximations for d/dx .” In: *Journal of Computational Physics* 110.1 (1994), pp. 47–67. doi: [10.1006/jcph.1994.1005](https://doi.org/10.1006/jcph.1994.1005).
- [75] M. Svärd and J. Nordström. “Convergence of energy stable finite-difference schemes with interfaces.” In: *Journal of Computational Physics* (2020), p. 110020. doi: [10.1016/j.jcp.2020.110020](https://doi.org/10.1016/j.jcp.2020.110020).

- [76] M. Svärd and J. Nordström. "On the convergence rates of energy-stable finite-difference schemes." In: *Journal of Computational Physics* 397 (2019), p. 108819. doi: [10.1016/j.jcp.2019.07.018](https://doi.org/10.1016/j.jcp.2019.07.018).
- [77] M. Svärd and J. Nordström. "Review of summation-by-parts schemes for initial-boundary-value problems." In: *Journal of Computational Physics* 268 (2014), pp. 17–38. doi: [10.1016/j.jcp.2014.02.031](https://doi.org/10.1016/j.jcp.2014.02.031).
- [78] P. E. Vincent, P. Castonguay, and A. Jameson. "A New Class of High-Order Energy Stable Flux Reconstruction Schemes." In: *Journal of Scientific Computing* 47.1 (2011), pp. 50–72. doi: [10.1007/s10915-010-9420-z](https://doi.org/10.1007/s10915-010-9420-z).
- [79] G. Yan, S. Kaur, J. E. Hicken, and J. W. Banks. "Entropy-stable Galerkin difference discretization on unstructured grids." In: *AIAA AVIATION 2020 FORUM*. 2020, p. 3033. doi: [10.2514/6.2020-3033](https://doi.org/10.2514/6.2020-3033).
- [80] H. Zhang, X. Qian, J. Yan, and S. Song. "Highly efficient invariant-conserving explicit Runge-Kutta schemes for nonlinear Hamiltonian differential equations." In: *Journal of Computational Physics* (2020), p. 109598. doi: [10.1016/j.jcp.2020.109598](https://doi.org/10.1016/j.jcp.2020.109598).